Earthquakes and Structures, *Vol. 17, No. 5 (2019) 521-532*
DOI: https://doi.org/10.12989/eas.2019.17.5.521

A new way to design and construct a laminar box for studying structure-foundation-soil interaction

X. Qin*, W.M. Cheung and N. Chouw

Department of Civil and Environmental Engineering. The University of Auckland, Auckland Mail Centre, Private Bag 92019, Auckland 1142, New Zealand

(*Received February 18, 2019, Revised August 27, 2019, Accepted October 15, 2019*)

Abstract. This paper describes the construction of a laminar box for simulating the earthquake response of soil and structures. The confinement of soil in the transverse direction does not rely on the laminar frame but is instead achieved by two acrylic glass walls. These walls allow the behaviour of soil during an earthquake to be directly observed in future study. The laminar box was used to study the response of soil with structure-footing-soil interaction (SFSI). A single degree-of-freedom (SDOF) structure and a rigid structure, both free standing on the soil, were utilised. The total mass and footing size of the SDOF and rigid structures were the same. The results show that SFSI considering the SDOF structure can affect the soil surface movements and acceleration of the soil at different depths. The acceleration developed at the footing of the SDOF structure is also different from the surface acceleration of free-field soil.

Keywords: laminar box; dynamic soil response; shake table test; structure-footing-soil interaction; soil boundary condition

1. Introduction

To experimentally study the dynamic behaviour of soil using a large volume soil specimen, a suitable method of containing the soil is required. Two types of container are commonly used, i.e., a rigid container and a shear box known as laminar box. A laminar box is the preferred option for most geotechnical earthquake engineering investigations. It is a flexible soil container. The ability to allow shear deformation during shaking, while at the same time to provide sufficient means of confinement, is a more realistic representation of the free-field boundary conditions of soil.

The design requirement of a laminar box has been discussed by many researchers (Huang *et al*. 2006, Wu *et al*. 2002, Bhattacharya *et al*. 2012, Pitilakis *et al*. 2008). Bhattacharya *et al*. (2012) summarized the need of a laminar box for a shake table test. Huang *et al*. (2006), Wu *et al*. (2002) evaluated the confinement effect of a laminar box on a soil specimen. It was concluded that the confinement provided by the laminar frame was effective in terms of simulating the soil confinement. Prasad *et al*. (2004) extended the study by performing further investigations on the influences of the laminar box. The activated inertia force of the laminar frame; the friction between laminar frames; and the effects of the waterproofing membrane were considered. It was concluded that all the aforementioned boundary effects had a negligible influence on the movement of the soil.

A number of studies have been conducted using laminar boxes to explore soil behaviour in earthquakes. Matsuda and Goto (1988) developed a lumped mass model to simulate the response of dry sand subjected to earthquake motion. The model was developed based on the findings from a shake table test with a laminar box. Ueng *et al*. (2006, 2010) used a bi-directional laminar box to determine the magnitude of sand settlement during earthquake motion. Using the experimental results, they developed mathematical correlations to predict the magnitude of sand settlement for both dry and liquefied sand. Krishna and Latha (2007) also adopted a small scale laminar box to investigate the seismic response of a soil retaining wall in relation to the relative density of the backfill. Laminar boxes have also been developed to simulate the interaction of soil and structural seismic response. Paolucci *et al*. (2008) conducted a large scale shake table test using a laminar box to validate the parameters for a numerical model of SFSI. A laminar box was also used to simulate the interaction between soil and an underground structure. Chen *et al*. (2010) used multiple laminar boxes to simulate the response of a utility tunnel under non-uniform earthquake excitation. Cubrinovski *et al*. (2006) performed a series of laminar box experiments to examine the response of piles under liquefaction induced lateral spreading. The effect of lateral spreading on pile foundations was also studied by Pamuk *et al*. (2007) using a laminar box.

Recently, a number of experimental studies in geotechnical engineering have been conducted using a transparent rigid sand box that allows the direct observation of soil behaviour during an earthquake. Anastasopoulos *et al*. (2007) conducted a centrifuge experiment to simulate the behaviour of fault rupture propagation through soil. To monitor the behaviour of soil during the development of

*Corresponding author, Ph.D.
E-mail: xqin009@aucklanduni.ac.nz

ISSN: 2092-7614 (Print), 2092-7622 (Online)

reverse and normal faulting, the walls of the sand container were made by perspex glass. The response of soil was obtained using a digital camera. Anastasopoulos *et al*. (2010) investigated the seismic performance of a bar-mat reinforced soil retaining wall using a relatively small scale sand box that was also transparent. In this instance, the advantage of using a transparent box was well illustrated. A similar experimental study has been performed by Sabermahani *et al*. (2009) to investigate the deformed shape of a retaining wall with reinforced soil. The effect of reinforcement length, spacing and stiffness on the seismic response of the retaining wall was studied. Zhou *et al*. (2018) studied the interaction between the soil and a tunnel structure due to earthquake. In their study, a rigid sand box was used. Qin and Chouw (2017) conducted a shake table experiment to simulate the soil structure interaction during aftershock earthquake.

Although it is known that a rigid transparent box cannot simulate the boundary condition of soil accurately, it nevertheless allows observation on the soil response rather than relying on instrumentation. On the other hand, laminar frames are constructed using metal members. Confining the specimen directly using the laminar frame will block the visualisation of soil within the box. A trade-off must be made between using a transparent rigid box and a laminar box.

In this study, a laminar box was designed and constructed that has transparency in the transverse direction. The confinement of soil in the transverse direction did not rely on the laminar frame. An acrylic glass wall was installed to achieve the transparency of a specimen. To evaluate the capability of the laminar box in simulating a realistic soil boundary condition, a shake table test was performed. The response of soil with three different configurations was studied. First of all, the response of sand with free-field conditions was considered. Secondly, a rigid structure was placed on the sand surface. Lastly, the rigid structure was replaced by a flexible SDOF structure. To enable a comparison of the results the total weight and the footing size of the rigid structure and those of the SDOF structure were kept the same. Furthermore, the laminar box was also used to investigate the effect soil boundary condition on the response of structure with SFSI.

2. Design requirement of soil container

The design of a soil container should be carried out in such a way that it can replicate as close as possible the stress-strain condition of an infinite lateral extent of soil profile. This is commonly achieved by using a laminar box. The principle use of a laminar box is to minimize the lateral stiffness of the container in order to ensure that the soil governs the response of the soil-box system. The soil in the laminar box can thus be excited by base excitations to simulate the dynamic response of soil during e.g., earthquake. An ideal laminar box should possess the following criteria (e.g., Wu *et al*. 2002):

1) Be able to simulate the correct free-field boundary conditions of the soil by providing sufficient confinement while being flexible to allow for shear deformation.
2) The laminar frame should be relatively light compared to the soil so that the inertia force of the frame activated during shaking will not affect the movement of the soil.
3) The laminar frames movement without soil should be free from friction.

The common design of a laminar box consists of a stack of laminar frames supported by bearings. The laminar frames are commonly constructed out of four rigid beams, or alternatively a circular ring. This means that the soil specimen will be completely confined by rigid components in all directions. The soil specimen itself is not visible.

3. Modified laminar box

Fig. 1 shows the laminar box constructed. The laminar layer was modified so that the soil specimen can be confined with the help of two Acrylic glass panels on two opposite sides. The overall dimension of the box is 1.28 m long, 1 m wide and 1.1 m high. It has the capacity to enclose a soil specimen with an internal dimension of 800 mm long by 800 mm wide by 700 mm high. The maximum allowable lateral movement of the laminar frame is ±70 mm in the longitudinal direction, resulting in a maximum soil shear strain of approximately 8%. The box was designed to facilitate a shear strain that covers the case of micro-tremors, i.e., a typical shear strain of the order of 10^{-6}, to the case of the epicentral zone of a large shallow earthquake where the shear strain in the near surface domain may reach 10^{-2} (Larkin 1978). Thus, the allowable lateral movement of the laminar frame provides an appropriate range for earthquake engineering applications.

As mentioned previously, the mass of the laminar frame will increase the horizontal inertia of the specimen, which will alter the soil response during an earthquake Prasad *et al*. (2004). Consequently, aluminium sections were used due to its relatively small mass while at the same time possessing sufficient stiffness to confine the soil specimen.

3.1 Laminar frame

The laminar box consists of 12 rectangular laminar frames. Fig. 2 shows the sketch of the top view of the

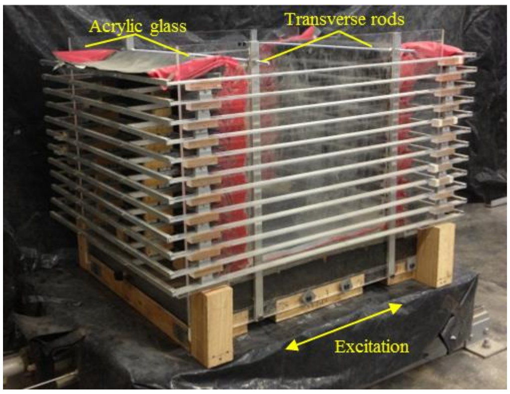

Fig. 1 The transparent laminar box

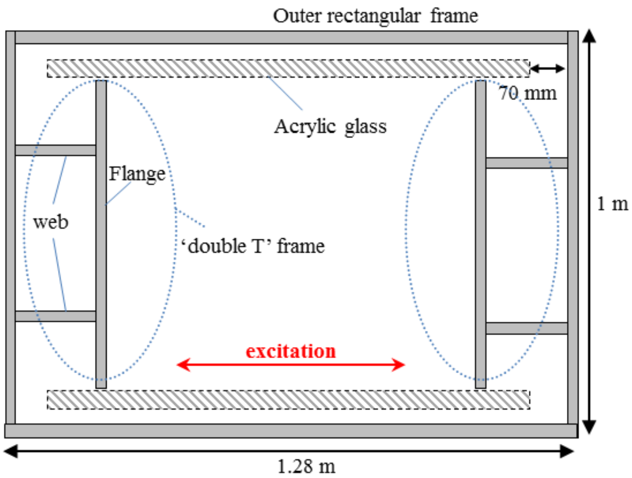

Fig. 2 Top view of the laminar frame

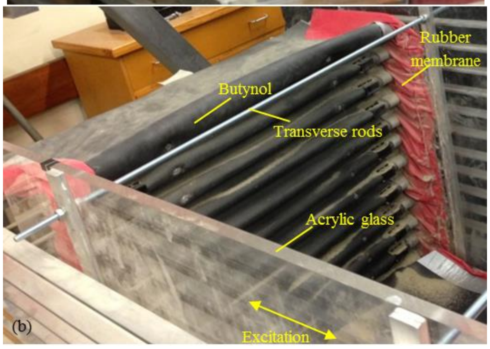

Fig. 3 Arrangement of the (a) ball bearings, and (b) the Butynol and the rubber membrane

laminar frame. Conventional laminar boxes are designed and constructed using a single rectangular or circular frame only (e.g., Wu *et al.* 2002, Bhattacharya *et al.* 2012, Pitilakis *et al.* 2008). The laminar frame in this study combined the rectangular frame with two 'double T' frames (circled in Fig. 2). The soil pressure in the excitation direction will act on the flange of the 'double T' frames and be transferred to the outer rectangular frame though the webs. To enclose the sides of the soil specimen, a sheet of acrylic glass was placed on each side of the 'double T' frame. The advantage is that the soil pressure in the transverse direction is not carried by the outer rectangular frame but by the two glass walls. The glass walls enable the specimen in the longitudinal direction to be viewed during an experiment. Transverse rods were perpendicularly passed through the glass walls, at both the top and the bottom, and secured with nuts (see Fig. 3(b)). The location of the acrylic glass panels are shown in Fig. 2. To avoid friction between the double *T* frame and the acrylic glass, a gap of approximately 1 mm was allowed. The gap was covered by a flexible membrane (presented later in the discussion of Fig. 3). The spacing between the end of the acrylic glass and the rectangular frame of the laminar is 70 mm (as shown in Fig. 2). This gap limits the maximum lateral displacement of the top laminar layer. This design is a simpler way to control the maximum lateral displacement of the box compared to what is utilised in many other designs (e.g., Wu *et al.* 2002, Bhattacharya *et al.* 2012, Pitilakis *et al.* 2008).

All members of the laminar frame were sized so that the maximum deflection under soil pressure was less than 0.1 mm. The soil pressure was calculated using dynamic passive pressure using the Mononobe-Okabe equation (Mononobe 1929, Matsuo and Ohara 1960, Lambe 1969). To avoid welding the aluminium components, the web and flange of the double *T* frame were post-tensioned to the outer rectangular frame using a threaded rod. It was found that this method can effectively connect the components while significantly reducing the cost.

Each laminar frame was stacked, one on top of the other and supported by 12 ball bearings to minimise the friction between the laminar frames. The ball bearings were located beneath the four webs of the double T frame and the corners of the outer rectangular frame (Fig. 3(a)). The gaps between the laminar were enclosed by a Butynol membrane. During shaking, the membrane must be able to deform such that the laminar can move freely, and hence the membrane was folded and then attached to the laminar as shown in Fig. 3. This configuration allows the laminar to move horizontally by utilizing the folding arrangement, while at the same time enclose any gaps between laminar layers. To provide a water-tight connection between the Butynol and the acrylic glass, a thin stretchable rubber membrane was used. The tensile stiffness of the rubber is much lower than that of the Butynol. This allows the rubber to stretch during shaking, but at the same time provides a barrier to prevent water and soil particles leaking from the box.

3.2 Preparation of the soil specimen

The laminar box was filed with 0.55 m of oven-dried river sand. To maintain a consistent relative density between experiments, the sand was rained into the laminar box from an initial height of approximately 1 m (Fig. 4(a)).

Rad and Tumay (1987) have identified the raining height required to form a uniform density of the soil specimen. In their investigation, they conducted a large number of sand raining experiments. Their results revealed that dry sand falling from a height greater than the terminal distance will produce sand specimens with similar relative densities. This terminal distance was suggested to be 300 mm. Since the raining height in the current study considerably exceeded 300 mm, the relative density was considered to be constant throughout the sand specimen. The raining procedure was repeated prior each experiment to achieve consistent initial soil properties. The total height

Table 1 Soil parameters

Parameters	Scale factor	SDOF structure
Mass (kg)	4800	19.2
Height (m)	15	0.59
Lateral stiffness (kN/m)	1200	7.3
Acceleration (g)	3.75	PGA/3.75
Earthquake duration (s)	2	10
Frequency (Hz)	0.5	3.2

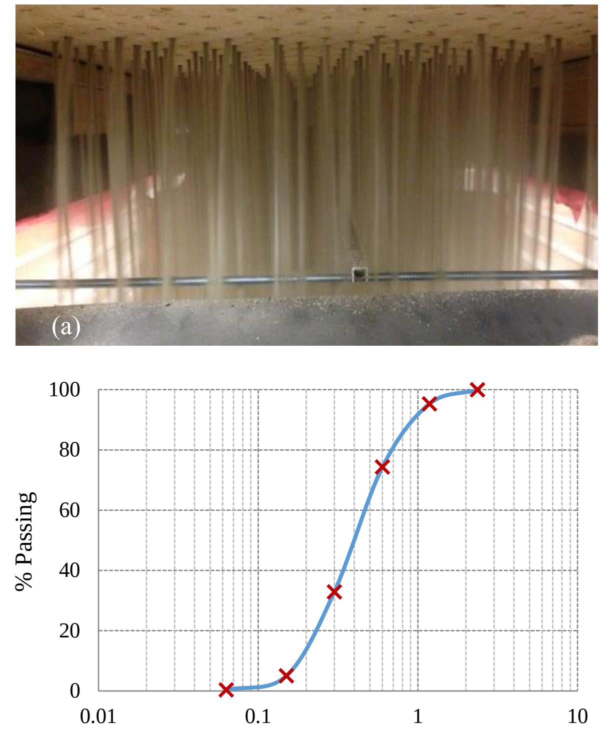

Fig. 4 Soil specimen (a) sand raining, and (b) particle size distribution

of the sand after each raining was 550±3 mm. The overall soil density between different tests was similar. Table 1 and Fig. 4(b) show the soil properties and particle size distribution of the sand specimen, respectively.

3.3 Resistance of the laminar box filled with sand

One of the major effects of a laminar box on the response of the sand specimen is the development of friction between the sand and the box structure. This friction between the sand grain and the confining box component can impede the soil movement during excitation. For this laminar box, the main source of this impediment is the friction between the acrylic glass and the sand. During shaking, the relative movement between the sand and the acrylic glass will cause energy loss through friction.

A push-over test was conducted on the sand-filled laminar box to quantify the box impediment to soil movement due to friction. Fig. 5(a) shows the test setup. A horizontal force was applied to a thick timber member via a load cell. The timber was included to ensure a uniform

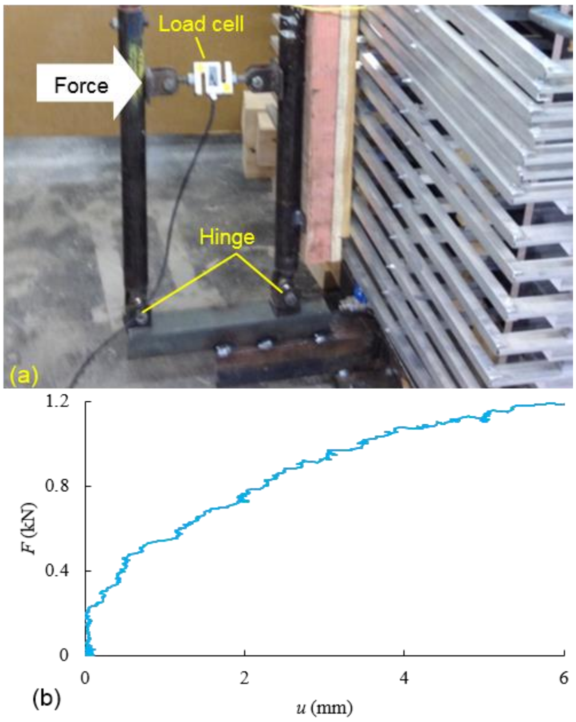

Fig. 5 Push-over test: (a) setup and (b) result

shear state in the laminar frames. The horizontal displacement at laminar layer corresponds to the soil surface was also measured. Based on the measured applied force (F) and the horizontal displacement (u), the friction resistance developed at the soil and glass wall interface can be estimated. Fig. 5(b) shows the result obtained from the push-over test. It is shown that the horizontal displacement at the soil surface did not take place until the applied horizontal force exceeds 0.2 kN. The result suggests that the resistance due to the friction at the soil and glass wall interface is 0.2 kN. As will be provided in Section 4.1, the lowest peak ground acceleration (*PGA*) of the considered excitations is 0.75 g. The horizontal force caused by a pseudo-static acceleration of this *PGA* is 5.2 kN. The friction force between the sand and the box structure is less than 5% of the applied horizontal force. The box impediment to the soil can be assumed as insignificant.

4. Shake table experiments

In this study, two sets of shake table experiments were conducted. The first set was conducted on sand with a free-field condition, to assess the capability of the laminar box in simulating the dynamic response of soil. In the second set of the experiments, the response of soil with SFSI was considered. Scale model structures based on the Buckingham π theorem (Buckingham 1914) were placed on the sand surface. The detail of the experiment will be discussed in detail in Section 6.

4.1 Ground excitation

The excitations utilized were ground accelerations

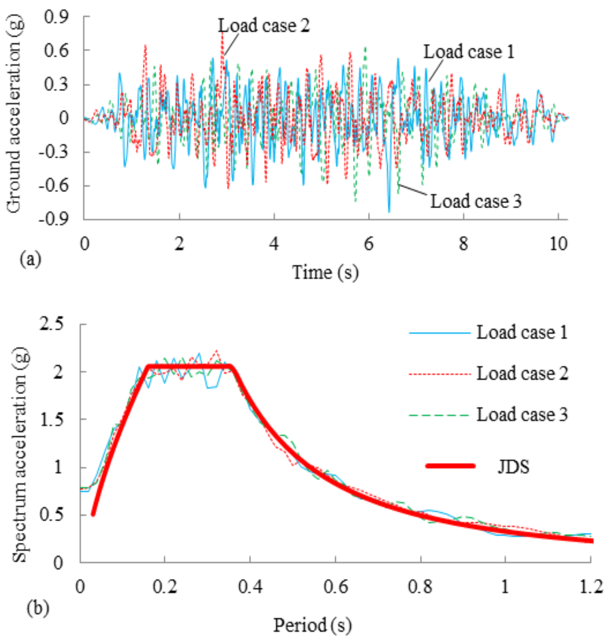

Fig. 6 Excitation (a) time history and (b) response spectrum

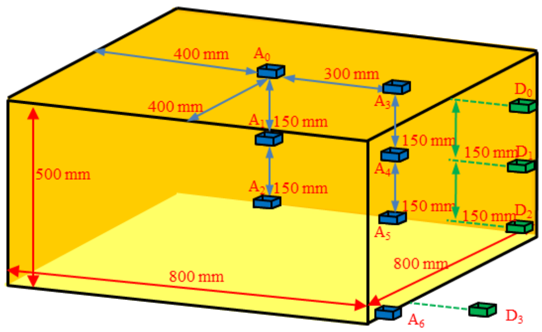

Fig. 7 Locations of instrumentations

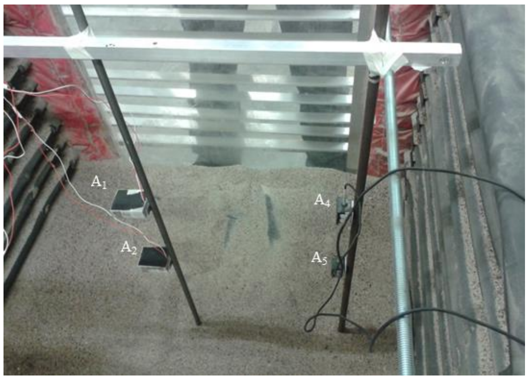

Fig. 8 Setup of the embedded accelerometers

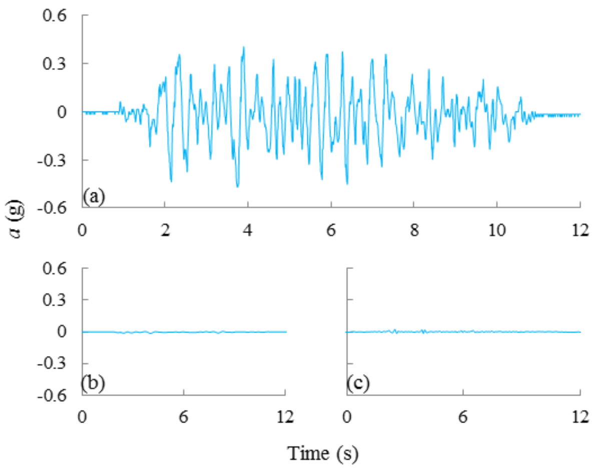

Fig. 9 Acceleration measured at A_1 location due to load case 2 in the (a) direction of excitation, (b) direction perpendicular to the excitation and (c) vertical direction

simulated based on of the Japanese Design Spectrum (JDS) (JSCE 2000) for a hard soil condition. The JDS was adopted due to their clearly defined frequency content. To comply with the scaling of the structure that is used later, the ground excitations were divided by the acceleration and time scale factors obtained from the Buckingham π theorem (1914). The scaled ground excitations are denoted as Load case 1-3 herein. The corresponding *PGA*s are 0.75, 0.78 and 0.79 g. Fig. 6(a) shows the acceleration time histories, and Fig. 6(b) shows the response spectra deduced from the three excitations using a 5% damping ratio.

4.2 Instrumentation

Fig. 7 shows the instrumentation in the soil specimen. In order to measure the acceleration at different locations in the specimen, seven accelerometers were used. Each of the two vertical profiles contains three accelerometers (A_0 to A_2 and A_3 to A_6), at a different depth location. Profile 1 (A_0 to A_2), was located along the centre-line of the surface of the specimen at depths of A_0=0, A_1=150 mm and A_2=300 mm. Profile 2 (A_3 to A_5) was located 300 mm away from profile 1. The depth of A_3 to A_5 was coincident with the depth of A_0 to A_2, respectively. A_1 and A_2 were three directional accelerometers, while the rest of the transducers were unidirectional accelerometers.

To avoid the sliding of surface accelerometers, A_0 and A_3 were separately attached to an aluminium plate which penetrated about 15 mm into the sand. A_1, A_2, A_4 and A_5 were suspended by a steel bar directly below the surface location of A_0 or A_3 prior to sand raining (Fig. 8). After the specimen was formed, the steel bars were carefully removed so that the accelerometers were embedded and could thus move freely with the sand.

An additional accelerometer (A_6) was attached externally to the base of the laminar box to measure the actual acceleration applied to the base of the box. Three draw-wire sensors (D_0 to D_2) were attached to the laminar frame in order to measure the lateral displacements at the boundary of the sand during shaking. These sensors were attached at a depth corresponding to those of the accelerometers (Fig. 7). An additional draw-wire sensor (D_3) was attached to the shake table.

Fig. 9 shows the three components of acceleration at the A_1 location due to Load case 2 (Fig. 7). As indicated, the acceleration in the out-of-plan (Fig. 9(b)) and vertical (Fig. 9(c)) directions were negligible compared to the acceleration in the direction of excitation (Fig. 9(a)). It can be concluded that the method introduced here allows a proper setup of accelerometers within the specimen.

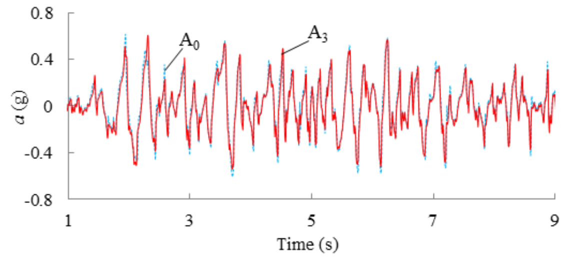

Fig. 10 Similar accelerations at the central region of the soil surface due to Load case 2

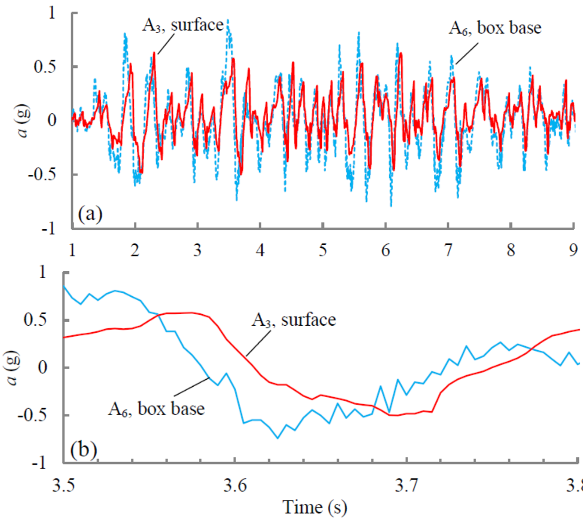

Fig. 11 Acceleration at the laminar box base and the sand surface due to load case 2 (a) time history and (b) in the time window of 3.5 s to 3.8 s

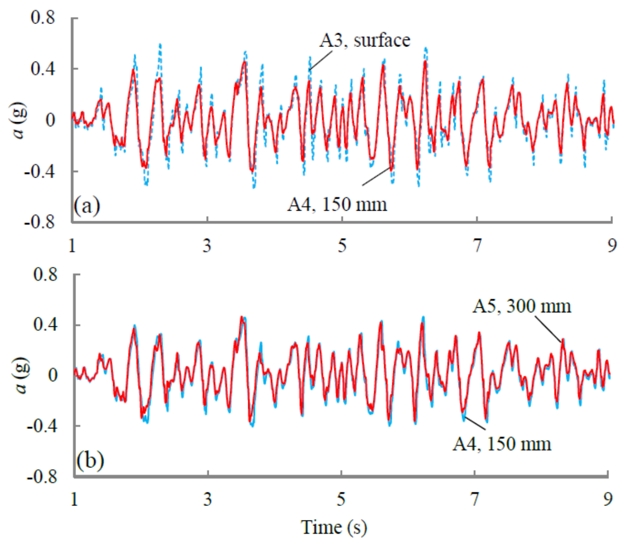

Fig. 12 Acceleration (a) on the surface and at150 mm depth and (b) at 150 mm and 300 mm depth due to Load case 2

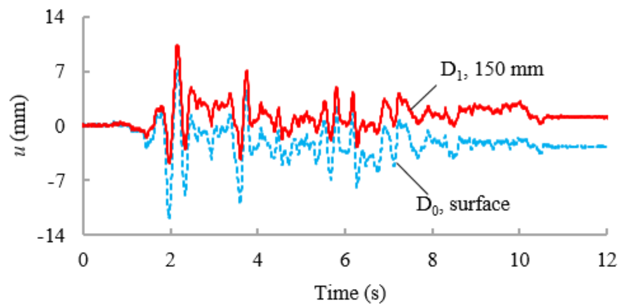

Fig. 13 Displacement of the laminar frame corresponds to different depths of the soil due to Load case 2

5. Free-field soil response

Fig. 10 shows the acceleration at different locations of the sand surface (A_0 and A_3), due to Load case 2, where the solid line corresponds to A_0 (at the centre of the surface) and the dashed line corresponds to A_3 (300 mm away from the centre). The two lines are almost identical, suggesting that the response of sand at different locations on a horizontal plane were almost the same. This indicates that the central region (within ±300 mm away from the centre) of soil can move homogenously during shaking. The influence of the laminar box on the response of soil in this domain is minimal. A similar observation can be made in the other two load cases.

Fig. 11 shows the acceleration of the sand surface (A_3) and that at the base of the box (A_6) during the Load case 2. The surface acceleration is significantly smaller than that at the base of the box. Since the box impediment of the soil movement is minimal, the alteration of the soil movement can be attributed to the material damping of the sand. The reduction of acceleration amplitude illustrates that there was a level of energy being dissipated as shear wave propagated through dry sand, revealing that significant damping occurred in the sand during the passage of the wave.

The amplitude of the high frequency component of the excitation was reduced due to soil material damping. This can be clearly observed in Fig. 11(b) in the time window between 3.5 s to 3.8 s. It was also found that there was a phase shift between the acceleration at the surface of the soil and shake table.

The accelerometers located on the surface (A_3), at 150 mm (A_4) and 300 mm (A_5) depths due to load case 2 were compared. As shown in Fig. 12(a), the acceleration at the surface of the soil (dotted line) was significantly larger than that at 150 mm depth of soil (solid line). The maximum acceleration at the surface of the soil was 0.6 g, while the acceleration at depths of 150 mm and 300 mm were respectively 0.46 g and 0.47 g. Although the maximum accelerations of A_4 and A_5 were similar to each other, the acceleration at 150 mm depth was often greater than that at a depth of 300 mm (Fig. 12(b)). The results in Figs. 11 and 12 indicate that compared to the acceleration at the base of the box, the sand accelerations were smaller. However, the sand accelerations increased with the decreasing depth location.

Fig. 13 shows the displacement (u) of sand at different depths. These displacements were obtained by the horizontal relative displacements between different depths of the soil and the shake table. On the surface of the soil (dashed line), the maximum relative displacement was 12.4 mm, equivalent to a shear strain of 2%. The residual relative displacement was 2.7 mm. The relative displacement highlights the advantage of utilising a laminar box in shake

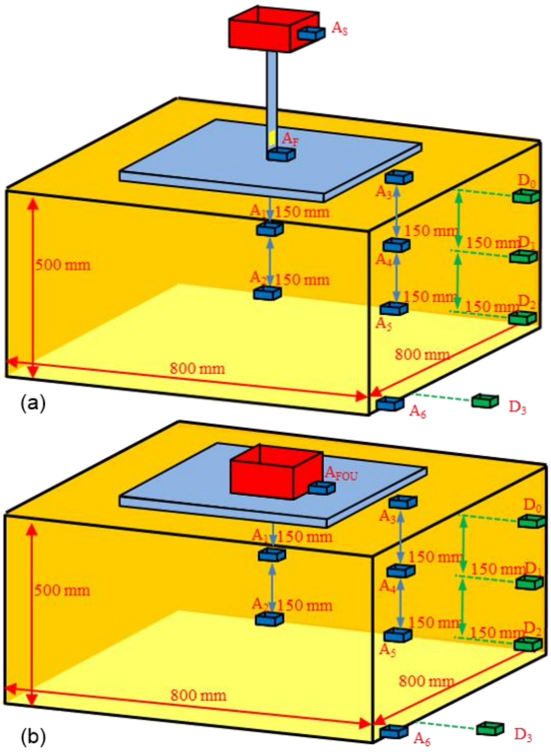

Fig. 14 Setup of a laminar box with (a) a SDOF structure and (b) a rigid structure

table testing. The ability to perform shear deformation in the soil specimen results in a more realistic free-field response of soil. The relative displacement achieved in the experiment, illustrates the excellent performance of this laminar box, with the capability to simulate the boundary conditions of free-field soil.

It is also found that the displacement of soil varied with depth. The maximum and residual horizontal displacements of sand at depth of 150 mm were 10.5 mm and 1.2 mm, respectively. These displacements were smaller than that found on the soil surface. However, at 150 mm depth, the maximum and residual displacements took place in the opposite direction to those at the soil surface. The results show that the response of box-soil system is driven by response of the soil but not the laminar box itself.

6. Response of structure-footing-soil system

To reveal the influence of SFSI on the response of sand, experiments involved model structures were conducted. Two structures were considered. i.e., a SDOF structure, obtained from a four storey structural prototype, and a rigid structure. The footing size and the mass of the rigid structure were the same as those of the SDOF structure (see Fig. 14). This ensured the effect of the weight imposed onto the soil due to different structures were the same.

6.1 Prototype and model scaling

The prototype considered was a four-storey building. The plan dimensions were 7 m by 7 m. The inter-storey height was 3.15 m with a total building height of 12.6 m. The structural elements were designed according to New Zealand design standards (NZS 2005). The building comprises of 170 mm concrete floor slabs, supported by 410UB54 steel beams. The columns were 310UC118, and these extended along the entire height of the building. A shallow footing with a mass of 29 tonnes was adopted. The footing was assumed to be rigid. The seismic mass was determined to be 29 tonnes for each floor and 25 tonnes for the roof. The fundamental period of the structure was 0.63 s. For simplicity the influence of higher modes is not considered. This was achieved by representing the prototype with an equivalent SDOF system. The effective height of the SDOF system is 8.9 m and the effective mass was 92 tonnes, representing 80% of the total mass of the prototype. The footing mass between the actual prototype and the equivalent SDOF system was kept the same.

Table 2 Scale factors for different model properties

Parameters	Scale factor	SDOF structure
Mass (kg)	4800	19.2
Height (m)	15	0.59
Lateral stiffness (kN/m)	1200	7.3
Acceleration (g)	3.75	PGA/3.75
Earthquake duration (s)	2	10
Frequency (Hz)	0.5	3.2

To comply with the shake table constraints, the SDOF system and the applied earthquake excitations were scaled down. To enable the measurements to reflect the prototype response, the scaling was needed by performing a dimensionless analysis. According to the Buckingham's π theorem (1914), any system consists of n number of physical variables and p number of physical quantities that can be expressed as a set of dimensionless group, π. In this study, the SDOF system can be characterised by three physical variables: mass of the prototype (m), geometrical dimensions (l), and lateral stiffness (k). In addition, the earthquake excitation can be characterised by another two physical variables: peak ground acceleration (a) and earthquake duration (t). The physical quantities in these variables are: mass (M), length (L) and time (T). This yields a total of five physical variables (n=5) and three physical quantities (p=3) in the system. The dimensionless groups, π, result from the dimensional analysis are presented in Qin (2016).

After considering the dimension and capacity of the shake table, the scale factor for l of 15 and m of 4800 were predefined. The time (t) was scaled by a factor of 2. Hence, the frequency of the constructed model will be two times that of the fundamental frequency of the prototype. The remaining scale factor for k and a was then determined by adapting the dimensionless group proposed in Qin *et al*. (2013). The scale factors for each variable are presented in Table 2.

The fundamental frequency of the SDOF structure was 3.2 Hz. A steel section was utilized to form the main supporting column. The thickness of the section was selected such that the fundamental frequency of the SDOF structure can be achieved. Note that the out-of-plane

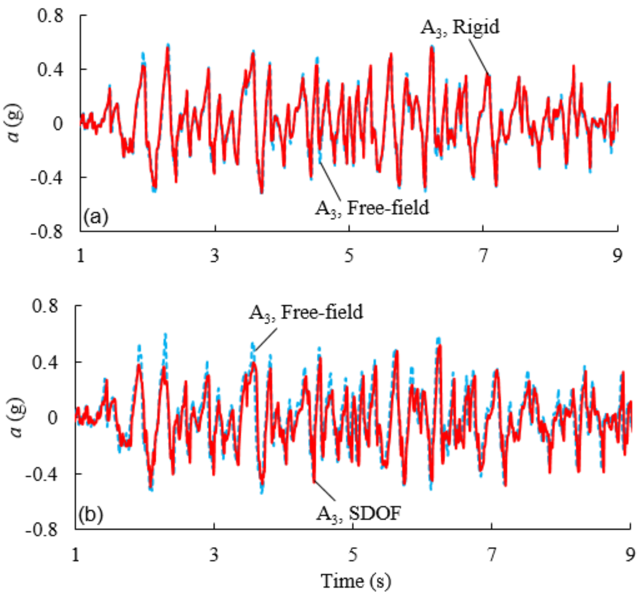

Fig. 15 Effect of SFSI due to (a) the rigid and (b) the SDOF structure

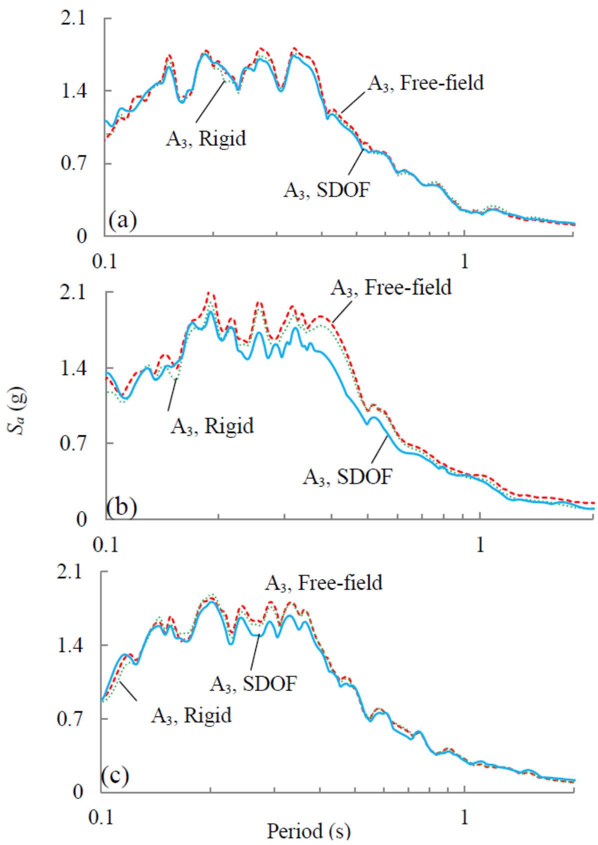

Fig. 16 Effect of SFSI on response spectra of the soil surface acceleration due to Load cases (a) 1, (b) 2 and (c) 3

stiffness of the column was defined to be rigid, because this study only focuses on the unidirectional shaking in the in-plane direction. The mass of this column was assumed negligible. The footing size was obtained by scaling down the footing dimension of the prototype, and this resulted in a plan dimension of 475 mm by 475 mm. Sand paper was attached to the bottom side of the footing to prevent sliding during shaking.

Another structure i.e., the rigid structure, with the same mass of the SDOF structure was also considered. The footing of the rigid structure was identical to that of the SDOF structure. This mass was achieved by attaching a piece of steel rigid block on the footing (Fig. 14(b)). The height of the centre of mass of the rigid structure (50 mm) was significantly lower than the height of the SDOF structure (590 mm). The rocking response of rigid structure can be neglected.

6.2 Experimental setup

The setups of considered structures on sand are shown in Fig. 14. When considering the SDOF structure (Fig. 14(a)), two accelerometers, denoted as A_S and A_F, were attached at the top mass and the footing of the structure, respectively. When the rigid structure was considered, one accelerometer (A_{FOU}) was attached to the footing of the structure (Fig. 14(b)). Strain gauge was attached at the column base of the SDOF model so that the base shear at the column during earthquake can be calculated.

6.3 Effect of SFSI on the acceleration at the soil surface

The acceleration (a) at the surface of soil, 300 mm away from the centre (indicated as A_3 location in Fig. 7) is shown in Fig. 15. Fig. 15(a) compares the case of soil with free-field (dotted line) and with the rigid structure (solid line) due to Load case 2. The rigid structure does not affect much of the acceleration on the soil surface. In contrast, when the SDOF structure was considered (Fig. 15(b)), the amplitude of the acceleration on the soil surface became smaller. The maximum acceleration at the soil surface with free-field condition was 0.61 g. With SFSI, i.e., considering the rigid structure and the SDOF structure, the corresponding maximum accelerations was 0.58 g and 0.52 g, respectively.

Fig. 16 shows the response spectra of the accelerations obtained on the soil surface (A_3), with and without structures. The response spectra were calculated using a 5% damping ratio. In the case of free-field soil and a rigid structure, the spectrum accelerations at the soil surface were similar. However, when the SDOF structure was considered, the spectrum value was smaller.

The slight variation of the frequency content of the ground excitation caused unequal SFSI which resulted in a variation of the reduction. Among the three excitations, considering Load case 2 gave the largest reduction. The reduction was most apparent between the periods of 0.18 s to almost 1 s When Load case 3 was considered, the reduction was observed between the period of 0.21 s and 0.38 s. In comparison, when Load case 1 was considered, this reduction was relatively small. It is logical to infer that SFSI will affect the response of surrounding soil.

Fig. 17 shows the time history of the horizontal acceleration at the top of the SDOF structure due to excitations considered. The response of the structure due to Load case 2 was the largest. The results confirmed that the

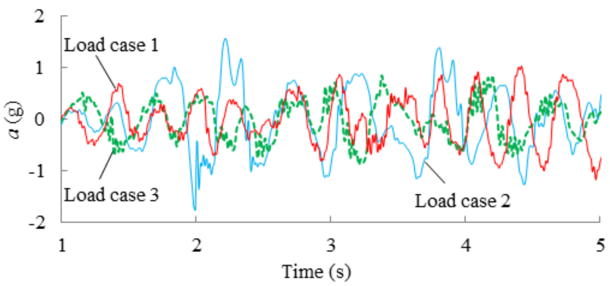

Fig. 17 Acceleration at the top of the SDOF structure

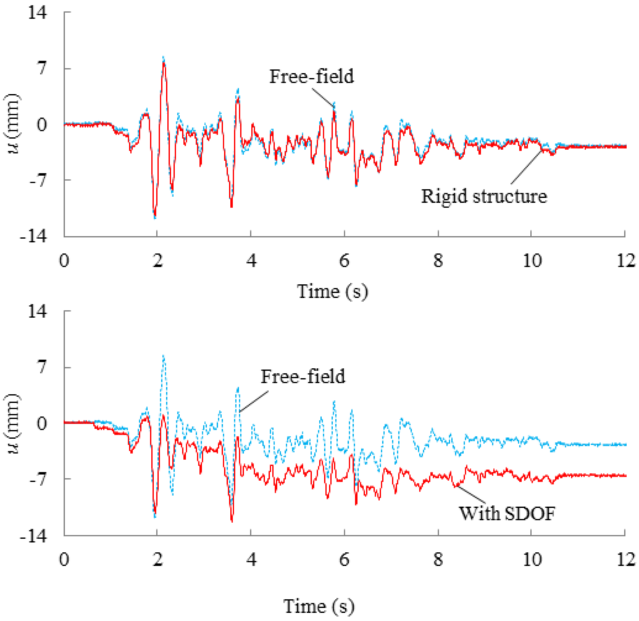

Fig. 18 Effect of SFSI on the soil displacement

stronger the response of the structure, the larger the reduction of the spectrum acceleration at the surface of the surrounding soil (see Fig. 16). The results show that SFSI can affect the response of surrounding soil. In case of closely adjacent structures, structure-soil-adjacent structure interaction is very likely to occur.

6.4 Effect of SFSI on the soil displacement

Figs. 18(a) and (b) reveal the effect of SFSI on the horizontal relative displacement of soil surface at the location A_3 due to the rigid and the SDOF structure, respectively. The horizontal displacement of soil surface with free-field and the rigid structure was very similar. When the SDOF structure was considered, the horizontal displacement of soil became larger. The maximum horizontal displacement of soil surface with free-field and a SDOF structure was 12.4 mm and 12.9 mm, respectively. At the end of the excitation, the residual horizontal displacement of the soil surface with free-field and a rigid structure were both approximately 2.7 mm. In contrast, the residual displacement of the soil surface with SFSI was 6.6 mm (Fig. 18(b)).

Fig. 19 plots the maximum horizontal displacement ($u_{\max}$) against the residual displacement of the soil surface for different experiments. For all cases, i.e., with and

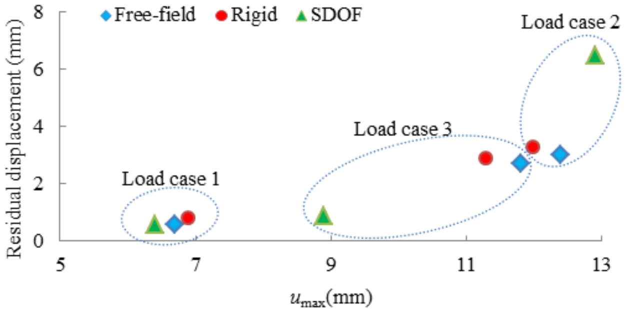

Fig. 19 Relationship between maximum and residual displacement of the soil surface at A_3 with and without structure

without structures, the residual displacement of soil increased with the maximum horizontal displacement. The maximum and residual displacements of the soil surface with the rigid structure were always similar to that on the free-field soil surface. On the other hand, when the SDOF structure was considered, the maximum displacement of the soil surface can become larger or smaller although the excitations for different load cases were simulated based on the same response spectrum (Fig. 6(b)). When Load case 1 was applied, the maximum displacement at the surface of soil with SFSI, was similar to that of the free-field condition. However, this was not the case when the other two load cases were considered. Compared to the maximum displacement of the soil surface with free-field condition and a rigid structure, the maximum displacement with the SDOF structure became larger and smaller in the case of Load cases 2 and 3, respectively. The residual displacement of soil surface was also affected by the response of the SDOF structure. For Load case 1, the residual displacement of soil with the SDOF structure was similar to the free-field and rigid structure case. In Load cases 2 and 3, the residual displacements of soil surface with SDOF structure were larger and smaller than those of free-field soil, respectively.

6.5 Acceleration in the structure

Fig. 20 compares the accelerations on the footing of the SDOF structure and that at the centre of the free-field soil surface. It can be seen that the acceleration at the footing is smaller than that at the free-field. Also, high frequency acceleration is evidenced at the footing of the structure. This high frequency acceleration can be attributed to the interaction between the soil, footing and the top mass. As observed during the experiments, partial footing of the SDOF structure separated from the supporting soil, i.e. footing uplift. The horizontal vibration frequency of the structure-footing-soil system during uplift increased. The high frequency vibration of the structure can also be observed in the time history of the horizontal acceleration at the top of the structure (Fig. 17). Because the uplift induced high frequency vibration in the structure-footing system, the frequency of footing acceleration during uplift also increased (Figs. 20(b) and (c)).

Fig. 21 shows the response spectra of accelerations at A_0, A_{FOU} and A_F locations. The dashed and solid lines

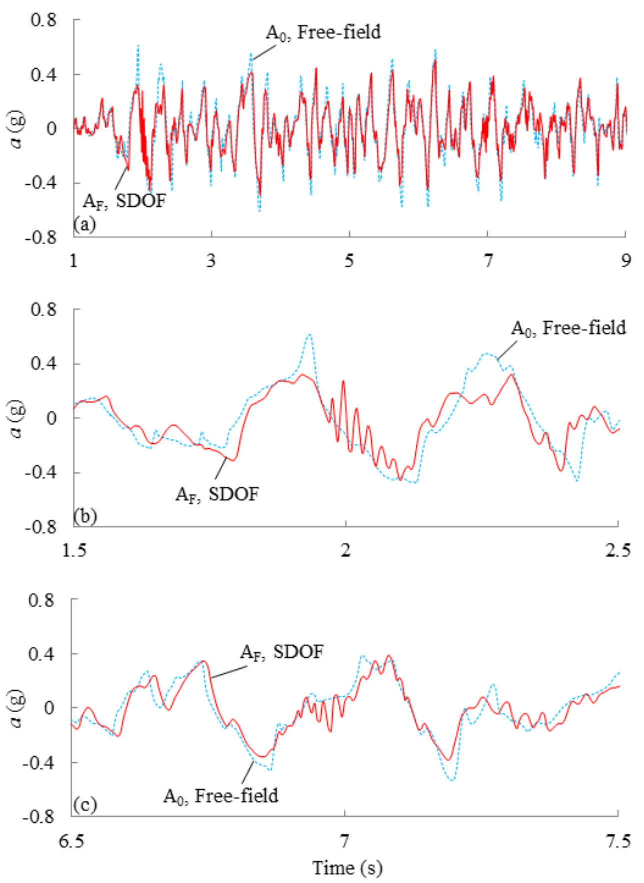

Fig. 20 Accelerations on the soil surface and at the structural footing due to load case 2: (a) time history and (b) and (c) at different time windows

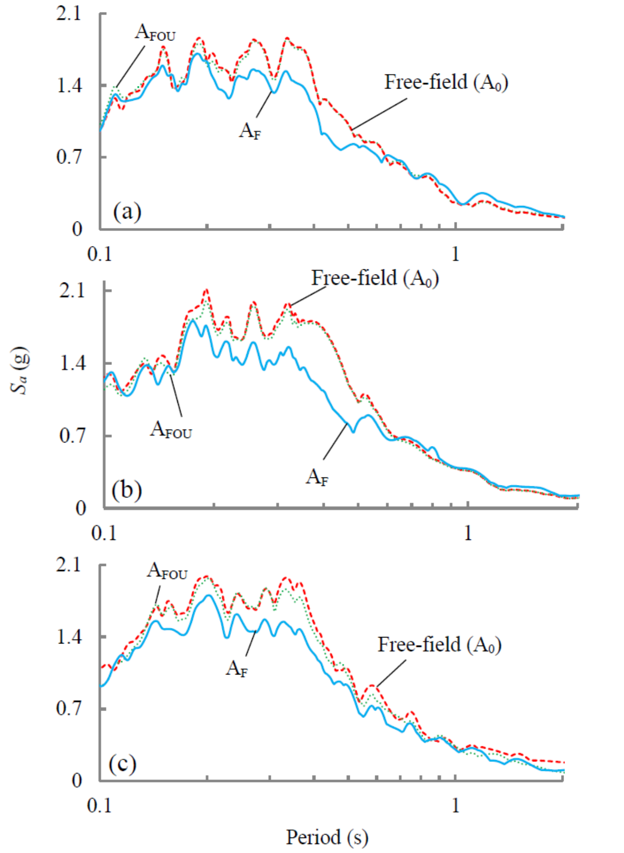

Fig. 21 Response spectra of acceleration on the soil surface and at the footing of rigid and SDOF structures due to (a) Load case 1, (b) 2 and (c) 3

represent the spectrum acceleration at the footing of the rigid and the SDOF structure, respectively. The dotted line shows the spectrum acceleration at the centre of the free-field soil surface. All spectra were calculated using a 5% damping ratio.

For all excitations, the response spectra of the accelerations on the footing of the rigid structure and free-field soil surface were similar. The spectrum accelerations at the footing of the SDOF structure were smaller than that at the free-field soil surface. Considering the SDOF structure, the spectrum values were generally the lowest. Especially at the region between 0.18 s and 0.6 s, the spectrum values at the footing of the SDOF were significantly lower than those of the other two cases. It should be noted that the fixed base fundamental period of the considered structure is 0.32 s. It is logical to infer that the reduction of spectrum values is associated with the dynamic properties of the structure.

At the location of the fundamental period of the structure, the spectrum values of the free-field soil condition are 1.84 g, 1.82 g and 1.96 g in the case of load case 1 to 3, respectively. For accelerations at the footing of the SDOF structure, the corresponding spectrum values are 1.50 g, 1.39 g and 1.50 g. The difference between the spectrum values obtained using surface acceleration of free-field soil and footing acceleration of structure shows the necessity of incorporating SFSI in the analysis of seismic response of the structure. In current seismic design, response of free-field soil is normally used as the excitation of the structure. The result obtained in this study indicates that free-field ground motion cannot appropriately represent the actual excitation of structure.

Chopra and Yim (1985) developed an equation of motion to calculate the response of a structure with a flexible support. The deformation of the support was modelled using a two-spring support. They developed a set of formulas to calculate the maximum base shear ($V_{\max}$) of structures on flexible supports

$$V_{\max} = V_{cr}\left\{\frac{h^2}{R_o^{\,2}} + e^{-\xi\phi}\sqrt{\frac{b^4}{R_o^{\,4}} + \frac{b^2}{R_o^{\,2}}\left[\left(\frac{\tilde{S}_a}{g}\right)^2\left(\frac{h}{b}\right)^2 e^{\xi\pi} - 1\right]}\right\} \quad (1)$$

where

$$\phi = \frac{\pi}{2} - \tan^{-1}\left\{\frac{b}{R_o}\left[\left(\frac{\tilde{S}_a}{g}\right)^2\left(\frac{h}{b}\right)^2 e^{\xi\pi} - 1\right]^{-1/2}\right\} \quad (2)$$

and b is half of the base width and h is the height of the model; g is the gravitational acceleration; $R_o = \sqrt{h^2 + b^2}$ and $V_{cr} = mg \times \frac{b}{h}$ is the base shear to initial footing uplift. $\tilde{S}_a$ is the spectrum acceleration corresponds to the effective vibration period $\tilde{T}$.

The effective vibration period of a structure with a flexible support is

$$\tilde{T} = T\sqrt{1+\frac{kh}{k_\theta}} \tag{3}$$

where T is the fundamental period of the structure with a fixed base, k is the lateral bending stiffness of structure and k_θ is the rotational assumed static stiffness of the footing on uniform soil:

$$k_\theta = \frac{G\pi}{8(1-\upsilon)}B^2 \tag{4}$$

where G and υ are the shear modulus and the Poissons ratio of the soil, respectively; B is the base width ($2b$).

An empirical equation was developed by Larkin (1978) such that the shear wave velocity (V_s) of sand can be calculated using the relative density (D_r), mass density (ρ) and mean effective confining stress (σ'_M)

$$V_s = \sqrt{\frac{D_r+25}{100}} \times \left[\frac{\sqrt{0.422\times 10^3 \times \sigma'_M}}{\rho}\right]^{0.5} \tag{5}$$

The shear wave velocity and can be used to calculate the shear modulus of soil

$$G = \rho V_s^2 \tag{6}$$

By combining Eqs. (5) and (6), Eq. (7) can be obtained to estimate the shear modulus (G) of sand using the relative density D_r and effective confining stress σ'_M.

$$G = \frac{D_r+25}{100} \times \sqrt{0.422\times 10^3 \times \sigma'_M} \tag{7}$$

The shear modulus of the sand at depth of 59 mm is 0.45 MPa. This depth, calculated from 1/8th of the footing width, is the appropriate depth for a characteristic soil element to represents the stress conditions of soil involved in providing resistance to moment and shear Larkin (2008). The effective vibration frequency of the model on sand is calculated to be 2.8 Hz (Eq. (3)). The effective vibration period of the model is very similar to the fixed base fundamental period. This is because the sand used in the experiment is not scaled. The high shear modulus of the sand results in a very high rotational stiffness of the footing.

Fig. 22 shows a comparison of the maximum base shear (V_{max}) of the model obtained using experimental data and Eq. (1). Strain gauge measurements are used to determine the maximum bending moment at the base of the model and thus the experimental maximum base shear can be calculated. The spectrum acceleration $\tilde{S}_a$ ($\tilde{T}$) is derived from the acceleration measured in the free-field soil surface (A_0 in Fig. 21). It can be seen that Eq. (1) overestimates the maximum base shear of the model. The experimentally obtained maximum base shear is 121.8 N. With Eq. (1), the average maximum base shears is 189.7 N. Eq. (1) overestimates the maximum base shear of model by 55.7%.

The accuracy of Eq. (1) is associated with the estimation of the effective vibration period of the model on sand. In the calculation of Eq. (3), the rotational stiffness of footing on soil is modelled using elastic springs. Footing uplift and soil plastic deformation are not considered. Therefore, the effective vibrational period of the model is underestimated.

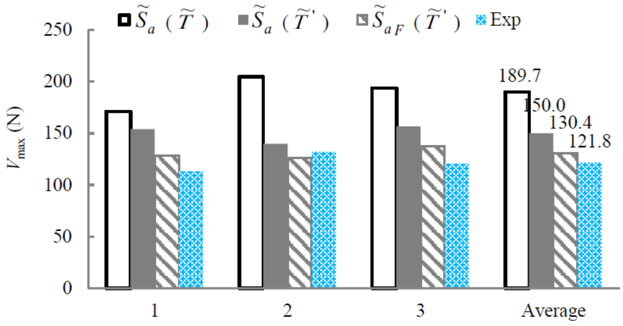

Fig. 22 Calculation of maximum base shear

Using the Fourier amplitude of the horizontal acceleration at the top of the structure, the frequency content of the structural response can be revealed. The maximum Fourier amplitude is found at 2.3 Hz, 1.88 Hz and 2.3 Hz for Load case 1 to 3, respectively. This indicates that the corresponding vibration periods ($\tilde{T}'$) are 0.43 s. 0.53 s and 0.43 s. Compared to the theoretical calculation ($\tilde{T}$= 0.36 s), Eq. (3) underestimates the effective vibration period. When $\tilde{T}'$ is used to obtain the spectrum value, the accuracy of Equation 1 can be improved. The maximum base shear of the model on average, estimated using $\tilde{S}_a$ ($\tilde{T}'$), is 150.0 N. Although Eq. (1) overestimates the maximum base shears by 23.2%, the calculations are closer to the experimental results. To further improve the accuracy of Eq. (1), the spectrum acceleration derived using footing acceleration (a_F or a'_F) in conjunction with $\tilde{S}_a$ can be used. The maximum base shear obtained from Equation 1 using $\tilde{S}_{aF}$ ($\tilde{T}'$) is 130.4 N. The corresponding errors reduce to 7%.

7. Conclusions

The design and construction a laminar box is presented. The advantage of the proposed design is that it allows visualization of the sub-surface soil as it is being excited by the shake table. The detail of constructing the laminar box is described. A procedure for setting up instruments in a soil specimen and an approach for achieving a uniform density of soil specimen in the box were presented. A series of shake table tests using three simulated excitations were conducted. The movement of soil at the central domain of the specimen appears to be unaffected by the laminar box. The box can confine the soil properly and realistically simulate the behaviour of soil during an earthquake.

Study on the effect of SFSI on the soil response considering free-field, and two structures i.e. a rigid and a SDOF structure reveals:

The response of soil with and without the rigid structure was similar. However, the presence of the SDOF structure can cause a smaller residual displacement at the soil surface.

SDOF structure causes a smaller spectrum acceleration of the soil near the structural footing.

The spectrum acceleration at the SDOF footing was smaller than that at the free-filed soil surface. The surface acceleration of free-field cannot represent the actual excitation of structures.

When comparing experimental results against those from an existing theoretical method, the accuracy of the method is sensitive to the effective vibration period of the SFSI system, and the spectrum acceleration of the footing.

Acknowledgments

The authors would like to thank the Ministry of Business, Innovation and Employment for the support through Natural Hazards Research Platform under the Award 3708936.

References

Anastasopoulos, I., Gazetas, G., Bransby, M.F., Davies, M.C.R. and El Nahas, A. (2007), “Fault rupture propagation through sand: finite-element analysis and validation through centrifuge experiments”, *J. Geotech. Geoenviron. Eng.*, **133**(8), 943-958. https://doi.org/10.1061/(ASCE)1090-0241(2007)133:8(943).

Anastasopoulos, I., Georgarakos, T., Georgiannou, V., Drosos, V. and Kourkoulis, R. (2010), “Seismic performance of bar-mat reinforced-soil retaining wall: Shaking table testing versus numerical analysis with modified kinematic hardening constitutive model”, *Soil Dyn. Earthq. Eng.*, **30**(10), 1089-1105. https://doi.org/10.1016/j.soildyn.2010.04.020.

Bhattacharya, S., Lombardi, D., Dihoru, L., Dietz, M.S., Crewe, A.J. and Taylor, C.A. (2012), “Model container design for soil-structure interaction studies”, *Role of Seismic Testing Facilities in Performance-Based Earthquake Engineering*, Springer Netherlands.

Buckingham, E. (1914), “Illustrations of the use of dimensional analysis”, *Phys. Simil. Syst. Phys. Rev.*, **4**(4), 354-377.

Chen, J., Shi, X. and Li, J. (2010), “Shaking table test of utility tunnel under non-uniform earthquake wave excitation”, *Soil Dyn. Earthq. Eng.*, **30**(11), 1400-1416. https://doi.org/10.1016/j.soildyn.2010.06.014.

Cubrinovski, M., Kokusho, T. and Ishihara, K. (2006), “Interpretation from large-scale shake table tests on piles undergoing lateral spreading in liquefied soils”, *Soil Dyn. Earthq. Eng.*, **26**(2), 275-286. https://doi.org/10.1016/j.soildyn.2005.02.018.

Huang, C., Zhang, H. and Sui, Z. (2006), “Development of large-scale laminar shear model box”, *Chin. J. Rock Mech. Eng.*, **25**, 2128-2134.

Japan Society of Civil Engineering (JSCE) (2000), Earthquake Resistant Design Code in Japan, Tokyo, Maruzen.

Krishna, A.M. and Latha, G.M. (2007), “Seismic response of wrap-faced reinforced soil-retaining wall models using shaking table tests”, *Geosyn. Int.*, **14**(6), 355-364. https://doi.org/10.1680/gein.2007.14.6.355.

Lambe, T.W. and Whitman, R.V. (1969), *Soil Mechanics*, Wiley, NY.

Larkin, T. (2008), “Seismic response of liquid storage tanks incorporating soil structure interaction”, *ASCE J. Geotech. Geoenviron. Eng.*, **134**(12), 1804-1814. https://doi.org/10.1061/(ASCE)1090-0241(2008)134:12(1804).

Larkin, T.J. (1978), “DENSOR- A computer program for seismic response analysis of nonlinear horizontal soil layers”, Report No 51508/6, Norwegian Geotechnical Institute.

Matsuda, T. and Goto, Y. (1988), “Studies on experimental technique of shaking table test for geotechnical problems”, *Proceeding of the 9th World Conference on Earthquake Engineering. Tokyo*, **8**, 837-842).

Matsuo, M. and Ohara, S. (1960), “Lateral earth pressures and stability of quay walls during earthquakes”, *Proceedings, Second World Conference on Earthquake Engineering*, Tokyo, Japan.

Mononobe, N. and Matsuo, O. (1929), “On the determination of earth pressure during earthquakes”, *Proceeding of the World Engineering Congress*, **9**, Tokyo.

NZS1170.5. (2004), Structural Design Actions Part 5: Earthquake Action, Standard New Zealand.

Pamuk, A., Gallagher, P.M. and Zimmie, T.F. (2007), “Remediation of piled foundations against lateral spreading by passive site stabilization technique”, *Soil Dyn. Earthq. Eng.*, **27**(9), 864-874. https://doi.org/10.1016/j.soildyn.2007.01.011.

Paolucci, R., Shirato, M. and Yilmaz, M.T. (2008), “Seismic behaviour of shallow foundations: Shaking table experiments vs numerical modelling”, *Earthq. Eng. Struct. Dyn.*, **37**(4), 577-595. https://doi.org/10.1002/eqe.773.

Pitilakis, D., Dietz, M., Wood, D.M., Clouteau, D. and Modaressi, A. (2008), “Numerical simulation of dynamic soil-structure interaction in shaking table testing”, *Soil Dyn. Earthq. Eng.*, **28**(6), 453-467. https://doi.org/10.1016/j.soildyn.2007.07.011.

Prasad, S.K., Towhata, I., Chandradhara, G.P. and Nanjundaswamy, P. (2004), “Shaking table tests in earthquake geotechnical engineering”, *Curr. Sci.-Bangalore*, **87**, 1398-1404.

Qin, X. (2016), “Experimental studies of structure-foundation-soil interaction effect on upliftable structures”, Doctoral Dissertation, ResearchSpace@ Auckland.

Qin, X. and Chouw, N. (2017), “Shake table study on the effect of mainshock-aftershock sequences on structures with SFSI”, *Shock Vib.*, **2017**, Article ID 9850915, 12. https://doi.org/10.1155/2017/9850915.

Qin, X. and Chouw, N. (2018), “Response of structure with controlled uplift using footing weight”, *Earthq. Struct.*, **15**(5), 555-564. https://doi.org/10.12989/eas.2018.15.5.555.

Qin, X., Chen, Y. and Chouw, N. (2013), “Effect of uplift and soil nonlinearity on plastic hinge development and induced vibrations in structures”, *Adv. Struct. Eng.*, **16**(1), 135-147. https://doi.org/10.1260/1369-4332.16.1.135.

Rad, N.S. and Tumay, M.T. (1987), “Factors affecting sand specimen preparation by raining”, *ASTM Geotech. Test. J.*, **10**(1), 31-37. https://doi.org/10.1520/GTJ10136J.

Sabermahani, M., Ghalandarzadeh, A. and Fakher, A. (2009), “Experimental study on seismic deformation modes of reinforced-soil walls”, *Geotext. Geomembran.*, **27**(2), 121-136. https://doi.org/10.1016/j.geotexmem.2008.09.009.

Ueng, T., Wang, M., Chen, M., Chen, C. and Peng, L. (2006), “A large biaxial shear box for shaking table test on saturated sand”, *Geotech. Test. J.*, **29**(1), 1-8. https://doi.org/10.1520/GTJ12649.

Ueng, T.S., Wu, C.W., Cheng, H.W. and Chen, C.H. (2010), “Settlements of saturated clean sand deposits in shaking table tests”, *Soil Dyn. Earthq. Eng.*, (1), 50-60. https://doi.org/10.1016/j.soildyn.2009.09.006.

Wu, X.P., Sun, L.M., Hu, S.D. and Fan, L.C. (2002), “Development of laminar shear box used in shaking table test”, *J. Tongji Univ.*, **30**(7), 781-785.

Zhou, H., Qin, X., Wang, X. and Liang, Y. (2018), “Use of large-scale shake table tests to assess the seismic response of a tunnel embedded in compacted sand”, *Earthq. Struct.*, **15**(6), 655-665. https://doi.org/10.12989/eas.2018.15.6.655.

CC